JOURNAL OF COLLOID AND INTERFACE SCIENCE 168, 217–221 (1994)

Light Scattering and Small-Angle Neutron Scattering Investigation for the L_1 Phase in a Ternary System

TOYOKO IMAE,*[,1] HIROSHI OKAMURA,* AND MICHIHIRO FURUSAKA†

*Department of Chemistry, Faculty of Science, Nagoya University, Nagoya 464, Japan; and †National Laboratory for High Energy Physics, Tsukuba, Ibaragi 305, Japan

Received December 15, 1993; accepted May 16, 1994

Light scattering and small-angle neutron scattering have been examined for the L_1 phase of dodecyldimethylamine oxide (C_{12}DAO)/hexanol/water system as a function of the mole fraction of hexanol, x. The molecular weight evaluated from light scattering increased from 1.54×10^4 at $x = 0$ to 20.4×10^4 at $x = 0.44$, while the hydrodynamic radii were 56 and 98 Å at $x = 0.33$ and 0.44, respectively. Guinier plots on small-angle neutron scattering decreased with downward curvature for solutions in the L_1 phase. An electron micrograph displayed the images of globular particles of 50–400 Å diameter, indicating the polydispersity in particle size. The numerical analysis based on the theoretical aspect for polydisperse spherical particles confirmed that molecular assemblies in the L_1 phase exhibited the bimodal distribution: spherical micelles of 44 Å diameter coexisted with microemulsions of 260 Å diameter, which were hexanol droplets stabilized by shells of surfactant molecules.

INTRODUCTION

Aqueous surfactant solutions undergo phase transition, when oils and/or cosurfactants are added. Interest for the phase behavior of multicomponent system can mainly be focused on the complicated phase diagram and the characterization of each phase. The phase behavior is important for practical applications such as oil recovery, drag delivery system, emulsified polymerization, photo chemistry reaction, coating technology, and so on (1–4). Therefore, the systems were investigated with various techniques including light scattering (LS), small-angle X-ray scattering (SAXS), small-angle neutron scattering (SANS), fluorescence spectroscopy, voltanometry, rheology, conductivity, and electron microscopy (5–16). Moreover, the physicochemical, especially thermodynamic, aspects were documented from an approach based on phenomenology and from a view of the nature of components and the geometric model of the microstructure (12, 17).

The phase diagram of the dodecyldimethylamine oxide (C_{12}DAO)/hexanol/water ternary system has been investigated at dilute concentrations of C_{12}DAO and hexanol (18). Six single phases were observed in the diagram. Each phase exhibited characteristic solution properties such as turbidity, irridescence, shear-anisotropy, and rheology. Electron microscopic observation was performed for C_{12}DAO/hexanol/water mixtures, and molecular assemblies were characterized in each phase (19). Characteristic properties of each phase were closely associated with the molecular assembly in the solution.

The L_1 phase with low hexanol content is transparent, fluid, and optically isotropic. The molecular assembly in this phase may be like spherical micelles which are formed in aqueous C_{12}DAO solutions. However, the fine structure of the assembly will be perturbed by the addition of hexanol. While overall size and shape of molecular assemblies can generally be estimated by LS investigation, SANS is suitable to characterize small particles, such as spherical micelles, and short distances, such as bilayer thicknesses (20, 21). In this work, the L_1 phase of the C_{12}DAO/hexanol/water system is examined by LS, SANS, and electron microscopy, and the fine structure of the molecular assembly in the L_1 phase is discussed.

EXPERIMENTAL

A sample of C_{12}DAO was purchased from Fluka. Extra pure grade hexanol is a commercial product. H_2O was redistilled from alkaline $KMnO_4$. D_2O (99.75%) was purchased from Wako Pure Chemical Industries, Ltd., and was utilized to prepare solutions for SANS measurement.

LS and specific refractive index increment were measured at 25°C on an Otsuka Electronics dynamic light scattering spectrophotometer DLS-700 and a differential refractometer RM102 by using a light of 488 nm wavelength. Details of measurement and analysis are described elsewhere (22).

SANS measurement was carried out at room temperature on a cold neutron small-angle scattering instrument WINK at the National Laboratory for High Energy Physics (KENS). The available wavelength λ of the spectrometer beam is 1–16 Å. Then 0.015–1 $Å^{-1}$ is the utilized magnitude of the

[1] To whom correspondence should be addressed.

0021-9797/94 $6.00

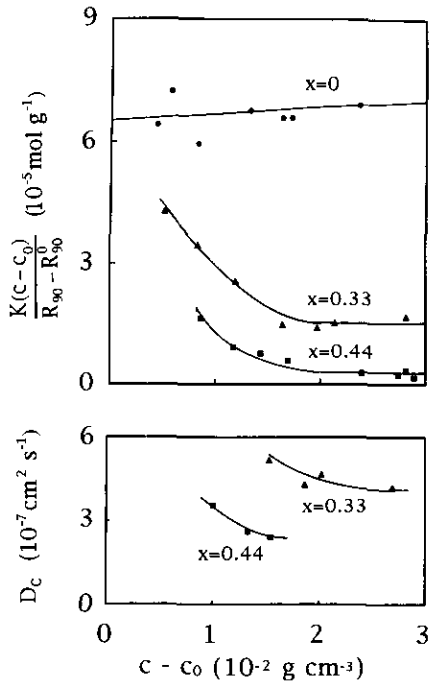

FIG. 1. Static and dynamic light scattering results for C_{12}DAO/hexanol/water mixtures at different mole fractions of hexanol, x: (upper) Debye plots at 90°; (lower) effective diffusion coefficients as a function of micellar concentration.

scattering vector $Q(=(4\pi/\lambda)\sin(\theta/2))$, where θ is the scattering angle. Samples were contained in a rectangular cell of $22 \times 40 \times 2$ mm.

Transmission electron microscopic (TEM) observation was performed at room temperature on a Hitachi H-800 electron microscope operated at 100 kV. The freeze-fracture replica films were prepared on a Balzers BAF 400 freeze-fracture device.

RESULTS

Static LS was measured for aqueous C_{12}DAO solutions at different mole fractions of hexanol, x. Significant angular dependence of light scattering was not observed for solutions at $x = 0$, 0.33, and 0.44. Figure 1 shows Debye plots at the scattering angle of 90°.

The Debye equation is described as

$$K(c - c_0)/(R_{90} - R_{90}^0) = 1/\mathrm{M} + 2B_2(c - c_0), \quad [1]$$

where K is the optical constant, R_{90} and R_{90}^0 are the reduced scattering intensities at 90° for solutions at surfactant concentration c and critical micelle concentration (CMC) c_0, respectively, and M and B_2 are the molecular weight and the second virial coefficient. The numerical value of CMC was obtained as a surfactant concentration where the reduced scattering intensity R_{90} began to increase.

The Debye plot for a solution at $x = 0$ increases with a positive slope. According to Eq. [1], the numerical values of M and B_2 were evaluated as 1.54×10^4 and 4.84×10^{-5} mol cm^3 g^{-2}, respectively. The numerical values of c_0, M, and B_2 were consistent with those previously reported (23). The evaluated aggregation number $m\,(=M/M_1) = 67$, where M_1 is the molecular weight of C_{12}DAO, indicates that the molecular assembly is spherical micelles.

The Debye plots for solutions at $x = 0.33$ and 0.44 decrease with micellar concentration $(c - c_0)$ and constrict to constant values at micellar concentrations above 2×10^{-2} g cm^{-3}, suggesting the variation from small micelles to large assemblies with micellar concentrations. The molecular weights at constant values were evaluated on the basis of Eq. [1], where the second virial coefficient was assumed to be negligibly small. The numerical values are listed in Table 1 with the corresponding values for a solution at $x = 0$. Table 1 includes values of specific refractive index increment $\partial\tilde{n}/\partial c$ and CMC. The molecular weight increases with increasing mole fraction of hexanol.

The effective diffusion coefficients D_c evaluated from dynamic LS at different scattering angles were numerically averaged and plotted in Fig. 1, since a meaningful angular dependence was not observed. The hydrodynamic radius R_H was calculated from

TABLE 1

Characteristics of Molecular Assemblies in the L_1 Phase of the C_{12}DAO/Hexanol/Water Ternary System at 25°C

	LS						SANS
x	$\partial\tilde{n}/\partial c$ (cm^3 g^{-1})	$10^2\,c_0$ (g cm^{-3})	C_0 (mM)	$10^{-4}\,M$	$10^7\,D_c$ (cm^2 s^{-1})	R_H (Å)	R_{max} (Å)
0	0.147	0.0589	25.7	1.54			22
0.29							22, 130
0.33	0.136	0.0589	25.7	10.3	6.40	56	
0.44	0.139	0.0589	25.7	20.4	5.30	98	22, 130

$$D_c = D_0\{1 + k_D(c - c_0)\} \approx D_0 = k_B T/6\pi\eta_0 R_H, \quad [2]$$

where D_0 is the translational diffusion coefficient. k_D is the hydrodynamic virial coefficient and is approximated to be null. k_B is the Boltzmann constant, T is the absolute temperature, and η_0 is the viscosity of solvent. Numerical values are included in Table 1. The hydrodynamic radii of 56 and 98 Å for molecular assemblies in solutions at $x = 0.33$ and 0.44 are larger than the estimated radius for spherical $C_{12}DAO$ micelles with a stretched hydrocarbon tail of surfactant.

SANS was measured for solutions at $x = 0$ (20, 50 mM $C_{12}DAO$), 0.29 (20 mM $C_{12}DAO$/8 mM hexanol, 50 mM $C_{12}DAO$/20 mM hexanol), and 0.44 (50 mM $C_{12}DAO$/40 mM hexanol). The Guinier plots are given in Figs. 2 and 3; while that for a solution at $x = 0$ displays a linear decrease with the square of the magnitude of the scattering vector Q, those for solutions at $x = 0.29$ and 0.44 decrease with downward curvature.

A TEM photograph is given in Fig. 4 for a mixture of $x = 0.29$ (50 mM $C_{12}DAO$/20 mM hexanol). The photograph presents images of globular particles with diameters of 50–400 Å.

DISCUSSION

Molecular assemblies formed in the L_1 phase of the $C_{12}DAO$/hexanol/water ternary system can be supported to be globular and polydisperse, as displayed by electron micrographs. The molecular weight and radius of globular particles estimated from light scattering are larger than those of spherical $C_{12}DAO$ micelles and increase with hexanol content.

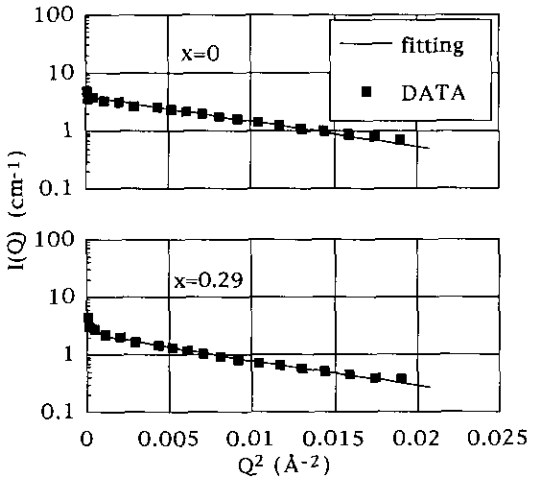

FIG. 2. Guinier plots of small-angle neutron scattering for $C_{12}DAO$/hexanol/water mixtures: (upper) $x = 0$ [20 mM $C_{12}DAO$]; (lower) $x = 0.29$ [20 mM $C_{12}DAO$/8 mM hexanol]. The solid line is the fitting curve for the theoretical analysis.

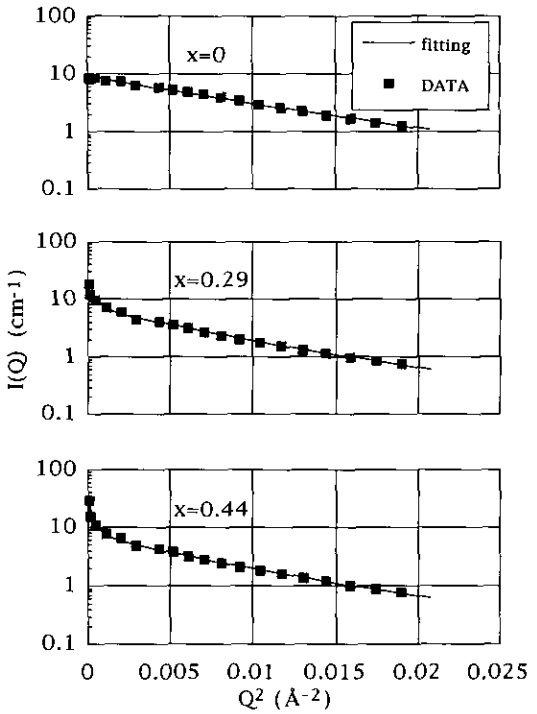

FIG. 3. Guinier plots of small-angle neutron scattering for $C_{12}DAO$/hexanol/water mixtures: (upper) $x = 0$ [50 mM $C_{12}DAO$]; (middle) $x = 0.29$ [50 mM $C_{12}DAO$/20 mM hexanol]; (lower) $x = 0.44$ [50 mM $C_{12}DAO$/40 mM hexanol]. The solid line is the fitting curve for the theoretical analysis.

The application of SANS analysis to polydisperse molecular assemblies was already reported. The polydispersity in size of the water core in a microemulsion of decane/AOT/D_2O was appreciable even at room temperature and increased with a rise of temperature (24). The size distribution was evaluated even for polydisperse rodlike micelles formed by short-chain lecithin (25).

When particles are not too large and the interaction between particles is negligibly small at low particle concentrations, the scattering vector dependence of neutron scattering intensity must mainly be contributed by the particle scattering factor. Then the scattering intensity of polydisperse particles is a sum of the contribution from an N-mer particle and is described by

$$I(Q) = \sum_{N=N_0}^{\infty} C_N N(b_m - \rho_S V_m)^2 \exp(-R_{G,N}^2 Q^2/3), \quad [3]$$

where C_N and $R_{G,N}$, respectively, are molar concentration and radius of gyration of an N-mer particle, and N_0 is the minimum aggregation number. b_m is the sum of the coherent neutron scattering length of a monomer, ρ_s is the coherent neutron scattering length density of the solvent, and V_m is the volume of monomer in a particle.

At the zero scattering vector,

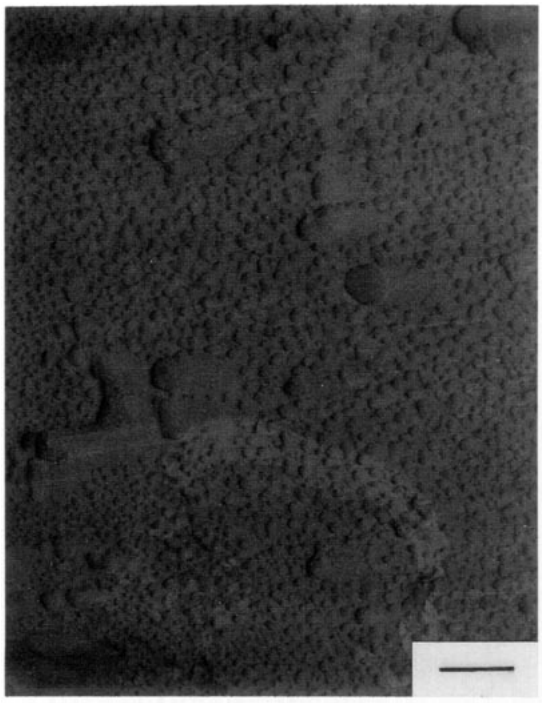

FIG. 4. TEM photograph for the 50 mM C_{12}DAO/20 mM hexanol/water (x = 0.29) system. The bar represents 200 nm.

$$\lim_{Q\to 0} I(Q) = I_0 = (b_m - \rho_S V_m)^2 \sum_{N=N_0}^{\infty} C_N N$$

$$= (b_m - \rho_S V_m)^2 (C - C_1)\bar{N}, \qquad [4]$$

and

$$C - C_1 = \sum_{N=N_0}^{\infty} C_N, \qquad [5]$$

where C and C_1 are the total and free monomer molar concentrations, respectively. C_1 can be equalized with the critical micelle concentration. $\bar{N}$ is the weight-averaged aggregation number and is described as follows:

$$\bar{N} = \sum_{N=N_0}^{\infty} C_N N / \sum_{N=N_0}^{\infty} C_N = \sum_{N=N_0}^{\infty} C_N N/(C - C_1). \qquad [6]$$

Then

$$I(Q) = I_0 \tilde{P}(Q) \qquad [7]$$

and

$$\tilde{P}(Q) = \sum_{N=N_0}^{\infty} [C_N N/(C - C_1)\bar{N}]\exp(-R_{G,N}^2 Q^2/3). \qquad [8]$$

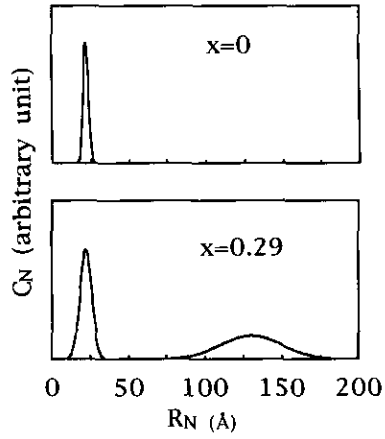

FIG. 5. The size distribution of molecular assemblies in C_{12}DAO/hexanol/water mixtures: (upper) x = 0 [20 mM C_{12}DAO]; (lower) x = 0.29 [20 mM C_{12}DAO/8 mM hexanol].

If particles are spheres with radius R_N,

$$R_{G,N}^2 = (3/5)R_N^2, \qquad [9]$$

$$NV_m = (4/3)\pi R_N^3, \qquad [10]$$

and

$$\tilde{P}(Q) = \sum_{N=N_0}^{\infty} [C_N N/(C - C_1)\bar{N}]\exp(-R_N^2 Q^2/5). \qquad [11]$$

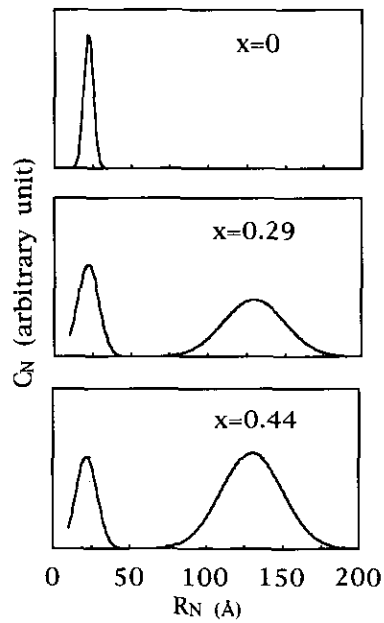

FIG. 6. The size distribution of molecular assemblies in C_{12}DAO/hexanol/water mixtures: (upper) x = 0 [50 mM C_{12}DAO]; (middle) x = 0.29 [50 mM C_{12}DAO/20 mM hexanol]; (lower) x = 0.44 [50 mM C_{12}DAO/40 mM hexanol].

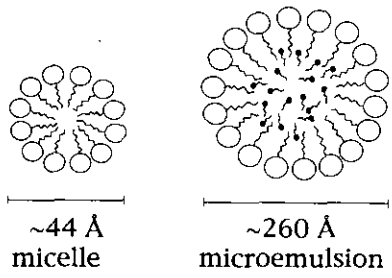

FIG. 7. · Schematic representation of a spherical micelle and a microemulsion.

Then

$$I(Q) = (b_m - \rho_S V_m)^2 \sum_{N=N_0}^{\infty} C_N N \exp(-R_N^2 Q^2/5). \quad [12]$$

Since concentrations of solutions examined in this work are low and close to CMC, the interparticle interaction may be small. Therefore, Eq. [12] can be applied to analysis of SANS results in Figs. 2 and 3. The set of C_N from C_{N_0} to C_∞ can be selected for particles with radius R_N from R_{N_0} to R_∞. The R_N value at each N was calculated from Eq. [10]. On the basis of Eq. [12], the optimum sets of C_N were determined by fitting the calculated $I(Q)$ curve to the observed one. These are plotted in Figs. 5 and 6 as a function of R_N, and the fitting curves are given in Figs. 2 and 3. The fitting curves were always satisfied the observed data. This means less contribution of the interaction term.

While C_N values for aqueous $C_{12}DAO$ solutions without hexanol displayed maximum at a certain R_N value, those for $C_{12}DAO$/hexanol/D_2O ternary systems showed two maxima, that is, the bimodal distribution. The R_N values with maximum C_N are listed as R_{max} in Table 1.

The numerical values of R_{max} were 22 and 130 Å. The smaller one is consistent with the radius of spherical $C_{12}DAO$ micelles. The fraction of larger particles increased with increasing mole fraction of hexanol. This suggests that larger particles are contributed by hexanol. Then larger globular particles could be assigned to be microemulsions which are hexanol droplets stabilized by shells of surfactant molecules, while smaller particles are regular spherical micelles. The schematic representation of models is given in Fig. 7. The possibility of the coexistence of a microemulsion and micelles was previously predicted by Israelachvili *et al.* (26).

Particle diameters of 50–400 Å estimated from electron micrographs comprise the distribution range of particle size evaluated from SANS (Figs. 5 and 6), although it should be taken into account that the preparation procedure of the replica film could cause overestimation of particle radii.

The numerical values of hydrodynamic radius R_H evaluated from light scattering are within two R_{max} values and increase with the mole fraction of hexanol, since those are the averaged ones. This indicates that SANS is a beneficial method to analyze components in the polydisperse system, while LS provides only the averaged values.

ACKNOWLEDGMENTS

This work was partly supported by the Hayashi Memorial Foundation for Female Natural Scientists. The authors are deeply indebted to Mr. T. Iwamoto and Mr. M. Ohsawa for their help with the electron microscopic observations and the small-angle neutron scattering measurements, respectively.

REFERENCES

1. Shah, D. O., and Schecter, R. S. (Eds.), "Improved Oil Recovery by Surfactant and Polymer Flooding." Academic Press, New York (1977).
2. Speiser, P., *in* "Reverse Micelles" (P. L. Luisi and B. E. Straub, Eds.). Plenum, New York, 1984.
3. Shah, D. O. (Ed.), "Macro and Microemulsions: Theory and Applications." Amer. Chem. Soc. Symposium Series, Vol. 272, Washington, DC, 1985.
4. Chew, C. H., and Gan, L. M., *J. Polym. Sci.* **23,** 225 (1985).
5. Chen, V., Warr, G. G., Evans, D. F., and Prendergast, F. G., *J. Phys. Chem.* **92,** 768 (1988).
6. Barnes, I. S., Hyde, S. T., Ninham, B. W., Derian, P.-J., Drifford, M., and Zemb, T. N., *J. Phys. Chem.* **92,** 2286 (1988).
7. Jahn, W., and Strey, R., *J. Phys. Chem.* **92,** 2294 (1988).
8. Lindmann, B., Shinoda, K., Jonströmer, M., and Shinohara, A., *J. Phys. Chem.* **92,** 4902 (1988).
9. Olsson, U., Nagai, K., and Wennerström, H., *J. Phys. Chem.* **92,** 6675 (1988).
10. Chokski, K., Qutubuddin, S., and Hussam, A., *J. Colloid Interface Sci.* **129,** 315 (1989).
11. Aoudia, M., Rodgers, M. A. J., and Wade, W. H., *J. Colloid Interface Sci.* **144,** 353 (1990).
12. Green, J. L., *J. Phys. Chem.* **94,** 5647 (1990).
13. Strey, R., Schomäcker, R., Roux, D., Nallet, F., and Olsson, U., *J. Chem. Soc. Faraday Trans.* **86,** 2253 (1990).
14. Uang, Y. J., Flaim, T. D., and Blum, F. D., *J. Colloid Interface Sci.* **139,** 381 (1990).
15. Schurtenberger, P., Magid, L. J., King, S. M., and Lindner, P., *J. Phys. Chem.* **95,** 4173 (1991).
16. Shubert, K.-V., and Strey, R., *J. Chem. Phys.* **95,** 8532 (1991).
17. Hyde, S. T., Ninham, B. W., and Zemb, T., *J. Phys. Chem.* **93,** 1464 (1983).
18. Platz, G., Thunig, C., and Hoffmann, H., *Ber. Bunsenges. Phys. Chem.* **96,** 667 (1992).
19. Imae, T., Iwamoto, T., Platz, G., and Thunig, C., *Colloid Polym. Sci.* **272,** 604 (1994).
20. Chen, S.-H., *Annu. Rev. Phys. Chem.* **37,** 351 (1986).
21. Chen, S.-H., and Lin, T.-L., *Methods Experimental Phys.* **23,** 489 (1987).
22. Imae, T., *J. Phys. Chem.* **94,** 5953 (1990).
23. Ikeda, S., Tsunoda, M., and Maeda, H., *J. Colloid Interface Sci.* **70,** 448 (1979).
24. Kotlarchyk, M., Chen, S.-H., and Huang, J. S., *J. Phys. Chem.* **86,** 3273 (1982).
25. Lin, T.-L., Chen, S.-H., Gabriel, N. E., and Roberts, M. F., *J. Phys. Chem.* **91,** 406 (1987).
26. Israelachvili, J. N., Mitchell, D. J., and Ninham, B. W., *J. Chem. Soc. Faraday Trans 2* **72,** 1525 (1976).